

VU Research Portal

A microbial role in the construction of Mono Lake carbonate chimneys?

Brasier, Alexander; Wacey, David; Rogerson, Mike; Guagliardo, Paul; Saunders, Martin; Kellner, Siri; Mercedes-Martin, Ramon; Prior, Tim; Taylor, Colin; Matthews, Anna; Reijmer, John

published in

Geobiology

2018

DOI (link to publisher)

[10.1111/gbi.12292](https://doi.org/10.1111/gbi.12292)

document version

Publisher's PDF, also known as Version of record

document license

Article 25fa Dutch Copyright Act

[Link to publication in VU Research Portal](#)

citation for published version (APA)

Brasier, A., Wacey, D., Rogerson, M., Guagliardo, P., Saunders, M., Kellner, S., Mercedes-Martin, R., Prior, T., Taylor, C., Matthews, A., & Reijmer, J. (2018). A microbial role in the construction of Mono Lake carbonate chimneys? *Geobiology*, 16(5), 540-555. <https://doi.org/10.1111/gbi.12292>

General rights

Copyright and moral rights for the publications made accessible in the public portal are retained by the authors and/or other copyright owners and it is a condition of accessing publications that users recognise and abide by the legal requirements associated with these rights.

- Users may download and print one copy of any publication from the public portal for the purpose of private study or research.
- You may not further distribute the material or use it for any profit-making activity or commercial gain
- You may freely distribute the URL identifying the publication in the public portal ?

Take down policy




If you believe that this document breaches copyright please contact us providing details, and we will remove access to the work immediately and investigate your claim.

E-mail address:

vuresearchportal.ub@vu.nl

ORIGINAL ARTICLE

A microbial role in the construction of Mono Lake carbonate chimneys?

Alexander Brasier¹  | David Wacey²  | Mike Rogerson³  | Paul Guagliardo² |
Martin Saunders² | Siri Kellner² | Ramon Mercedes-Martin³ | Tim Prior³ |
Colin Taylor¹ | Anna Matthews⁴ | John Reijmer^{5,6}

¹School of Geosciences, University of
Aberdeen, Aberdeen, UK

²University of Western Australia, Perth, WA,
Australia

³University of Hull, Hull, UK

⁴BP Exploration, Sunbury on Thames, UK

⁵KFUPM Saudi Arabia, Dhahran, Saudi
Arabia

⁶VU University Amsterdam, Amsterdam, The
Netherlands

Correspondence

Alexander Brasier, School of Geosciences,
University of Aberdeen, Aberdeen, UK.
Email: a.brasier@abdn.ac.uk

Funding information

Australian Research Council, Grant/Award
Number: FT140100321; BP Exploration
Co, Grant/Award Number: GPTLIBPXIMB/
NB/89573; Deutscher Akademischer
Austauschdienst

Abstract

Lacustrine carbonate chimneys are striking, metre-scale constructions. If these were bioinfluenced constructions, they could be priority targets in the search for early and extraterrestrial microbial life. However, there are questions over whether such chimneys are built on a geobiological framework or are solely abiotic geomorphological features produced by mixing of lake and spring waters. Here, we use correlative microscopy to show that microbes were living around Pleistocene Mono Lake carbonate chimneys during their growth. A plausible interpretation, in line with some recent works by others on other lacustrine carbonates, is that benthic cyanobacteria and their associated extracellular organic material (EOM) formed tubular biofilms around rising sublacustrine spring vent waters, binding calcium ions and trapping and binding detrital silicate sediment. Decay of these biofilms would locally have increased calcium and carbonate ion activity, inducing calcite precipitation on and around the biofilms. Early manganese carbonate mineralisation was directly associated with cell walls, potentially related to microbial activity though the precise mechanism remains to be elucidated. Much of the calcite crystal growth was likely abiotic, and no strong evidence for either authigenic silicate growth or a clay mineral precursor framework was observed. Nevertheless, it seems likely that the biofilms provided initial sites for calcite nucleation and encouraged the primary organised crystal growth. We suggest that the nano-, micro- and macroscale fabrics of these Pleistocene Mono Lake chimneys were affected by the presence of centimetre-thick tubular and vertically stacked calcifying microbial mats. Such carbonate chimneys represent a promising macro-scale target in the exploration for ancient or extraterrestrial life.

1 | INTRODUCTION

Distinguishing biologically influenced sedimentary rock structures from abiotic ones in the field, or when selecting high priority targets from remote images, is a key challenge in the search for early and extraterrestrial life. There are few recognisable millimetre to decimetre-scale structures identifiable as definitively “microbial” in outcrop. Free-standing chimneys composed of

carbonate, sulphate or silicate minerals, if requiring the influence of organisms to develop, provide a potential set of targets for terrestrial geological and astrobiological investigation (e.g., Walter & Des Marais, 1993).

Mono Lake, California, is a globally important site for studying potential biogeochemical processes creating “tufa” limestone chimney constructions around sublacustrine vents. It is renowned for its Pleistocene to twentieth-century vegetation-encrusting tufa,

found aligned along faults associated with springs and boulder-encrusting tufa sheets on the lake margins (Dunn, 1953; Russell, 1889). These impressive, tower-like structures are only the most recent phase of lacustrine carbonate deposition that has been occurring sporadically within Mono Lake at least since the last glaciation (Wang et al., 2014). Although together these features are considered an archetypal carbonate-precipitating hyperalkaline lacustrine environment (Della Porta, 2015), their depositional mechanisms are surprisingly little studied. This is in part because no active carbonate mineral precipitation has been reported since sporadic events in the 1980s and early 1990s, when ikaite ($\text{CaCO}_3 \cdot 6\text{H}_2\text{O}$) and gaylussite ($\text{Na}_2\text{Ca}(\text{CO}_3)_2 \cdot 5\text{H}_2\text{O}$) were reportedly forming where spring waters mixed with lake waters along the southern shore of the lake (Bischoff, Stine, Rosenbauer, Fitzpatrick, & Stafford, 1993; Stine, 1987).

Both geochemical and geobiological models have been put forward in an attempt to explain voluminous past tufa formation in Mono Lake. In the purely geochemically driven models, it is postulated that calcium carbonate precipitation was caused by mixing of carbonate-rich, high pH lake water with Ca-rich spring water (Cloud & Lajoie, 1980; Dunn, 1953; Rieger, 1992). Similar models have recently been invoked to help explain sublacustrine chimneys of the Afar Rift (Dekov et al., 2014). A popular geochemical model for Mono Lake contends that the dominant primary-formed carbonate mineralogy is ikaite (Bischoff et al., 1993), and that in most cases, this later recrystallises to gaylussite (Bischoff et al., 1993) or calcite (Council & Bennett, 1993). Mound and chimney morphologies in these geochemical models are explained by mineral precipitation from upward rising, low-density sublacustrine plumes of spring waters. However, such chimneys have not actually been demonstrated to spontaneously form under sterile conditions, and turbulent mixing zones between water masses may produce powder-like mineral precipitates in the water column (consistent with the “milky white” spring waters observed by Stine, 1987) rather than coherent benthic constructions. Macrocrystalline, benthic sheets of calcite in other contexts require the presence of a benthic biofilm (cf. Pedley, Rogerson, & Middleton, 2009).

Early geobiological models were based on observations of microbes or algae at sites of active tufa growth that were inferred to have influenced carbonate precipitation (Scholl & Taft, 1964). Given the enormous dissolved inorganic carbon (DIC) pool in Mono Lake and high pH such that the majority of this DIC is present as carbonate, postulated photosynthetic effects on carbonate mineral deposition are likely to be negligible (cf. Arp, Reimer, & Reitner, 2001). Stable carbon isotopes of Mono Lake tufa samples record temporal variations in the bulk lake water DIC that relate to changes in plankton productivity and burial (Li & Ku, 1997). However, no study has yet reported any local $\delta^{13}\text{C}_{\text{calcite}}$ enrichment relative to lake average that could be attributed to photosynthetic CO_2 uptake at the site of carbonate precipitation. Instead, a more logical microbial mechanism for carbonate mineral formation is via binding of calcium by the copious amounts of extracellular organic material (EOM)

produced by cyanobacteria (Emeis, Richnow, & Kempe, 1987), with calcification taking place during or following calcium release on heterotrophic EOM breakdown (Arp, Hofmann, & Reitner, 1998; Arp, Thiel, Reimer, Michaelis, & Reitner, 1999; Arp et al., 2001; Dupraz, Visscher, Baumgartner, & Reid, 2004). We follow others including Dupraz, Fowler, Tobias, and Visscher (2013) in using the broader term EOM rather than EPS (extracellular polymeric substances) here because EOM encompasses all organic matter external to the cell, including low molecular weight organic carbon, not just the larger EPS molecules.

An alternative geobiological model for carbonate chimney growth in Mono Lake might be calcite replacement of a microbially precipitated clay precursor, as has been proposed for thrombolitic microbial carbonates of Lake Clifton, Australia (Burne et al., 2014) and dolomitic microbialites of Great Salt Lake, United States (Pace et al., 2016). Pertinent to this model was a report of potential microbial mediation of magnesium silicate growth within calcite-cemented clastic lake sediment (locally known as “sand tufa”; Cloud & Lajoie, 1980) on the southern shore of Mono Lake (Souza-Egipsy, Wierzbos, Ascaso, & Nealson, 2005). In these lake sands, however, no evidence for calcite precipitation around living or decaying microbes was found (Souza-Egipsy et al., 2005).

Geomorphologically, mound and column structures are well known to arise under the influence of photosynthetic (cf. stromatolites and thrombolites) and chemosynthetic (black and white smoker) microbial activity, with the biofilm providing a focus for mineral growth and directly promoting benthic carbonate mineral sheet formation (Bosak et al., 2012; Kempe et al., 1991; Petroff, Beukes, Rothman, & Bosak, 2013; Reid et al., 2000).

Here, we provide new *in situ* macro- to nanoscale evidence for the participation of microbes in the construction of Mono Lake chimneys and argue that the location and morphology of the Mono Lake tufa chimneys is a result of a complex interplay between lake dynamics (faults, venting of sublacustrine springs, lake chemistry) and the benthic microbial communities within the lake.

2 | METHODS

2.1 | Fieldwork and sample processing

Fieldwork around Mono Lake was undertaken in October 2014. Samples were taken with permission of the Mono Lake Tufa State Natural Reserve following their guidelines and under their supervision. It was a requirement of the permit that only the minimum required number of naturally broken samples should be taken. Several different occurrences of tufa carbonate rocks were examined around the lake, but the most interesting were Pleistocene chimney structures close to Mono City (Figures 1, 2a) that are the focus of this article. Possible microbial influence on construction of these chimneys was noted in the field (Figure 2), based on mat-like sheets that connected chimney pipes (Figure 2b). The locations of the chimneys as determined by GPS are linearly arranged, presumably along a fault. Indeed faults mapped

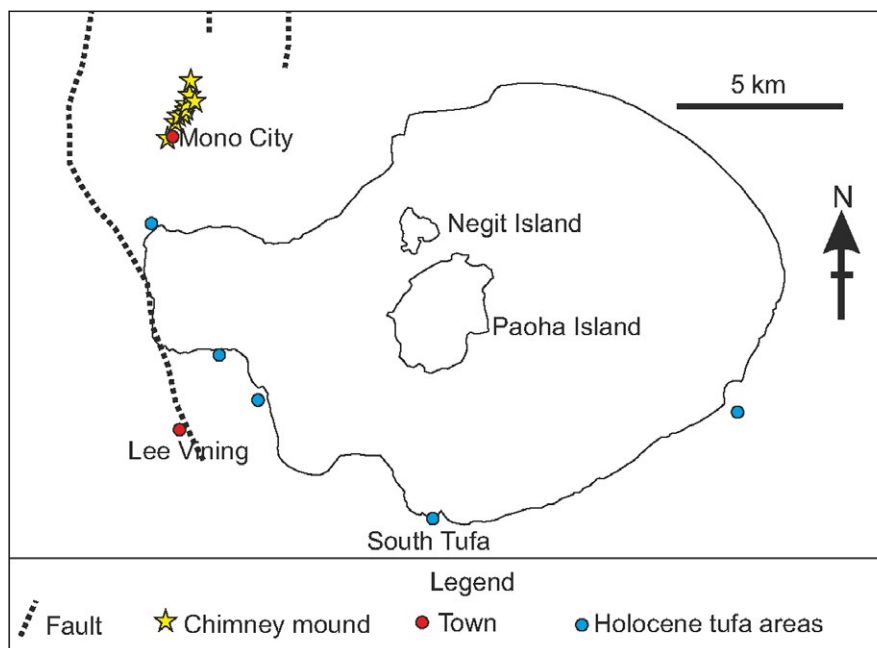


FIGURE 1 Map of Mono Lake, California. Pleistocene chimney mounds of the Mono City area described in this article are yellow stars in the northwest corner. Other areas known for the more widely reported Holocene tufa carbonates are shown as blue circles. Towns of Lee Vining and Mono City are shown as red circles. Scale bar is 5 km [Colour figure can be viewed at wileyonlinelibrary.com]

by Jennings, Strand, and Rogers (1977) run parallel to the line of the Pleistocene chimneys (Figure 1). Further laboratory work was aimed at determining whether the central chimney pipes were solely abiotic or microbially influenced in origin. For this, a representative (naturally broken) sample that was clearly from the centre of a chimney was sent to VU University Amsterdam. Pipe material was cut up and pieces were consolidated by impregnation with blue-stained epoxy resin so that several thin sections could be made. Very high abundance of organic filaments was apparent in each of these pipe wall thin sections (described and illustrated further below). A large number (>10) of thin sections of this pipe material were optically examined and then sent to the Centre for Microscopy, Characterisation and Analysis at the University of Western Australia. One representative thin section was selected for NanoSIMS, FIB-SEM and TEM analyses to test (i) whether the filaments were genuine microfossils, and (ii) to determine spatial relationships between cell walls and minerals, which might help to determine whether these purported microbes influenced chimney growth form.

2.2 | XRD analysis

Three subsamples of the same specimen from which the thin sections were produced were crushed for XRD analysis at the University of Hull. X-ray powder diffraction data were collected from ground samples mounted in stainless steel sample holders. Analysis was performed on a PANalytical Empyrean X-ray diffractometer (XRD) operating in Bragg-Brentano geometry using copper $K\alpha_1$ radiation ($\lambda = 1.540546 \text{ \AA}$) and a PIXEL detector.

Each data set was the sum of three identical data collections with $4 \leq 2\theta/^\circ \leq 100$, a step size of 0.02626° and counting time 1,140 s per step.

2.3 | Biomarker analysis

Biomarker analysis was conducted on a further off-cut of the Pleistocene tufa chimney specimen used for XRD analysis and microscopy. This was done in the organic geochemistry laboratory at the University of Aberdeen. The sample was first cleaned with Dichloromethane. It was then crushed and Soxhlet extracted using a Dichloromethane/Methanol mixture (93:7). The extract was analysed on an Agilent 6890GC with an Agilent 5975MS. The GC column was a 30 m long * 0.25 mm i.d. * 0.25 μm film thickness GC-5 column. The gas chromatography temperature programme was 60°C for 2 min, heating at 20°C per minute up to 120°C , then at 4°C per minute up to 290°C and holding for 27.5 min.

2.4 | Focussed ion beam (FIB) preparation of TEM samples

Prior to FIB preparation, resin-embedded polished geological thin sections were examined by optical microscopy, using Zeiss Axioskop 2 and Leica DM2500M microscopes, plus scanning electron microscopy (SEM), using a FEI Verios XHR SEM, in order to gain an understanding of filament distributions and morphologies, and to select the most appropriate targets for detailed study. A dual-beam FIB system (FEI Helios NanoLab G3 CX) at the Centre for Microscopy, Characterisation and Analysis, University of Western Australia

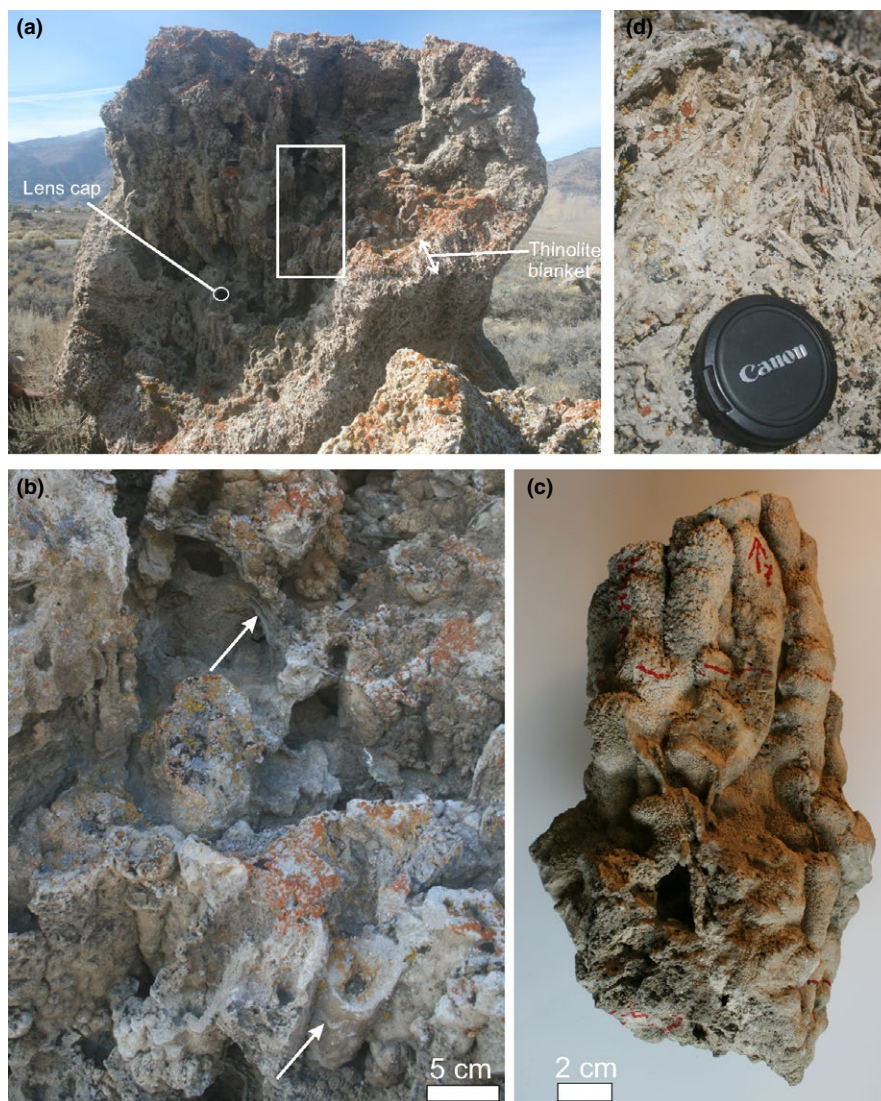


FIGURE 2 Field images of Mono City tufa chimneys. (a) One of the chimneys standing erect on former lake floor sediments and coated in a blanket of “thinolite” (pseudomorphs after ikaite, labelled). Lens cap for scale is circled. (b) Close-up of pipes in the chimney from the boxed area in (a). Lower arrow points to the exterior of one of the cylindrical pipes that makes up the chimney structure, and upper arrow points to calcitic mat-like structure bridging between pipes. (c) Specimen of pipes on which further microscale analyses were undertaken. (d) Close-up of thinolite blanket on the exterior of one of the chimneys, showing these pseudomorphs after ikaite have a very different appearance from the underlying chimney construction illustrated in (b) and (c) [Colour figure can be viewed at wileyonlinelibrary.com]

was then used to prepare ultrathin TEM wafers from the thin sections coated with c. 20 nm of gold. Electron beam imaging within the dual-beam FIB was used to identify previously mapped microstructures of interest in the thin sections allowing site-specific TEM samples to be prepared. The TEM sections were prepared by a series of steps involving different ion beam energies and currents (see Wacey, Kilburn, Saunders, Cliff, & Brasier, 2011 for details); after initial thinning to c. 1 μm the wafers were extracted using an *in situ* micromanipulator and welded onto PELCO FIB-lift-out Cu TEM grids. Final thinning to c. 150 nm was then done *in situ* on the grid using lower beam currents. FIB preparation of TEM sections allows features below the surface of the thin sections to be targeted, thus eliminating the risk of surface contamination producing artefacts.

Distinction between the epoxy resin used in sample preparation and other organic materials was possible via NanoSIMS ion mapping (see below).

2.5 | TEM analysis of FIB-milled wafers

TEM data were obtained using a FEI Titan G2 80-200 TEM/STEM with ChemiSTEM Technology operating at 200 kV, located within the Centre for Microscopy, Characterisation and Analysis, University of Western Australia. Data obtained included bright-field TEM images, HAADF (high angle annular dark field) STEM images, EDS (ChemiSTEM) maps and selected area electron diffraction patterns for mineral identification.

2.6 | SEM-EDS

SEM-EDS was performed on the *FEI Helios Nanolab G3 CX* instrument at the Centre for Microscopy, Characterisation and Analysis, University of Western Australia which is equipped with an *Oxford Instruments X-Max 80* energy dispersive X-ray spectroscopy (EDS) system and *Oxford Instruments AZtec 3.0* nanoanalysis software. All analyses were performed on FIB-milled faces below and perpendicular to the surface of the thin sections to avoid surface contamination.

2.7 | NanoSIMS ion mapping

NanoSIMS ion mapping was performed using a *CAMECA NanoSIMS 50* at the Centre for Microscopy, Characterisation and Analysis, University of Western Australia, with instrument parameters optimised as described in Wacey et al. (2011). Analysis areas varied from $22 \times 22 \mu\text{m}$ up to $35 \times 35 \mu\text{m}$, at a resolution of 256×256 pixels (each pixel measuring between 86 nm and 137 nm, depending on the size of the area imaged). Dwell times were 30 ms per pixel with a beam current of c. 1.3 pA ($D1 = 3$). Secondary ions

mapped were $^{16}\text{O}^-$, $^{24}\text{C}_2^-$, $^{12}\text{C}^{14}\text{N}^-$, $^{28}\text{Si}^-$, $^{24}\text{Mg}^{16}\text{O}^-$ and $^{56}\text{Fe}^{16}\text{O}^-$, and charge compensation was achieved using the electron flood gun. In all cases, regions c. 2–5 μm larger than the intended analysis area were pre-sputtered with the primary ion beam (using c. 17 pA beam current; $D1 = 1$) to $>5 \times 10^{16}$ ions/ cm^2 to remove surface contamination, implant Cs^+ ions and reach a steady-state of ion emission. NanoSIMS data presented were produced in one session, but to enable measurement of six different ions with the *CAMECA NanoSIMS 50* each area was analysed twice, with one detector retuned between analyses. For each area, analysis one was O, C, CN, Si, FeO, and analysis two was O, C, CN, MgO, FeO. Differences in the relative intensities of the $^{24}\text{C}_2^-$ versus $^{12}\text{C}^{14}\text{N}^-$ maps are partly due to the higher ionisation potential of the secondary ion $^{12}\text{C}^{14}\text{N}^-$; here we report only the $^{12}\text{C}^{14}\text{N}^-$ maps because of the higher secondary ion yield and the fact that $^{24}\text{C}_2^-$ is also found in the carbonate minerals surrounding the organic material. $^{12}\text{C}^{14}\text{N}^-/^{24}\text{C}_2^-$ ratios were used to identify epoxy resin introduced during sample preparation based on previous data showing that the epoxy possesses significantly lower $^{12}\text{C}^{14}\text{N}^-/^{24}\text{C}_2^-$ than that of biological cell walls or potential extracellular organic material (Wacey, Gleeson, & Kilburn, 2010).

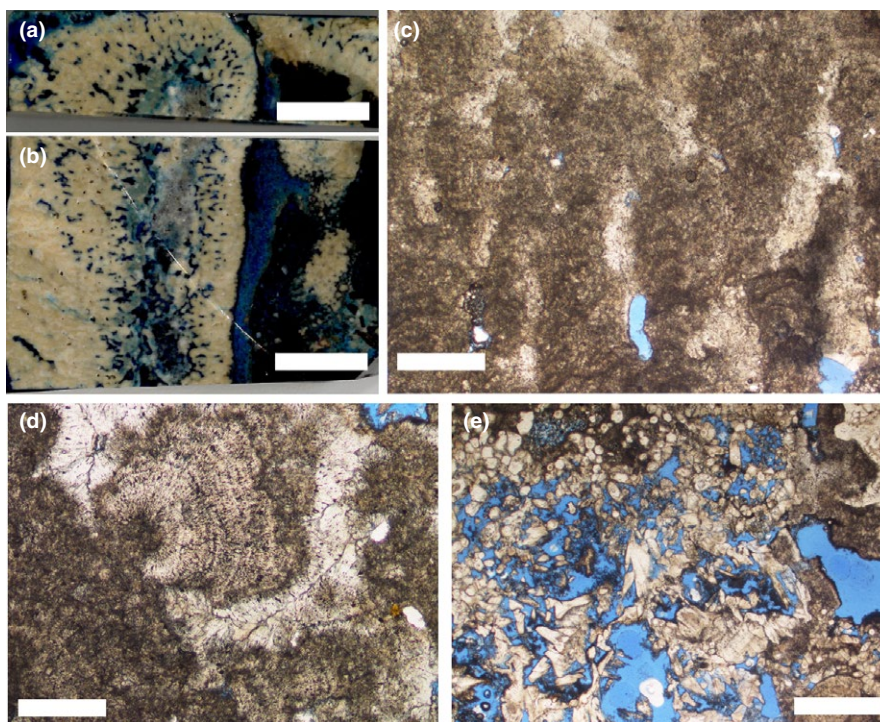


FIGURE 3 Petrography of Mono City chimneys. (a) Transverse cut and (b) longitudinal cut through one cylindrical chimney pipe. The specimen was impregnated with blue resin, so blue areas were void space in the rock. Axis of the pipe is the (blue resin impregnated) vertical cavity to the left of centre of (b). Space between pipes is also filled with blue resin. (c) Thin section of pipe wall under plane polarised light showing it comprises columns of laminated micritic calcite separated by partially spar-filled voids (white where spar-filled, blue resin where empty). (d) A shrub-like calcite microspar crystal fan surrounded by clear white spar and nucleated on darker micrite. The micrite and shrub-like fan in particular are full of dark inclusions (microbial filaments). (e) Inclusion-free crystals best interpreted as pseudomorphs after euhedral ikaite (Shearman et al., 1989), now calcite, are distinctively different from the pipe wall material. The high porosity results from the significant volume change on transformation from ikaite to calcite. Scale bars are 10 mm for (a and b), 1 mm for (c, e) and 500 μm for (d) [Colour figure can be viewed at wileyonlinelibrary.com]

3 | RESULTS

Our study aimed to determine whether Mono Lake chimneys are purely physicochemical constructions, or whether microbes influenced their development. We focus on chimneys found north of the present lake at Mono City, on a Pleistocene lake terrace (Zimmerman, Hemming, Hemming, Tomascak, & Pearl, 2011) at around 2,065 m altitude, extending along a 2.25 km long N to NNE oriented line interpreted as a fault trace (Figure 1). The late Pleistocene Mono City chimneys reported and described here are older than the more commonly studied and illustrated mounds of presumed Holocene and younger age found close to

the modern shoreline in the southeast (South Tufa) and northeast (Boardwalk area) of the lake (Figure 1). A sample of a Holocene fallen block from the Lee Vining area on the southwest shore of the modern lake was also analysed by XRD for comparison with the Pleistocene materials.

The Mono City chimneys vary from c. 3 to 4 m in height, and from c. 1.5 to 3 m in width (Figure 2a). Internally the chimneys are constructed of stacks of numerous calcitic cones or pipes, each 30–60 cm in height and around 3 cm in width (Figure 2a–c). Each pipe has a central 1 cm-sized void or conduit (Figures 2b, 3a,b). The outsides of these pipes are commonly coated in botryoids of calcite (confirmed by XRD) that range from 0.5 to

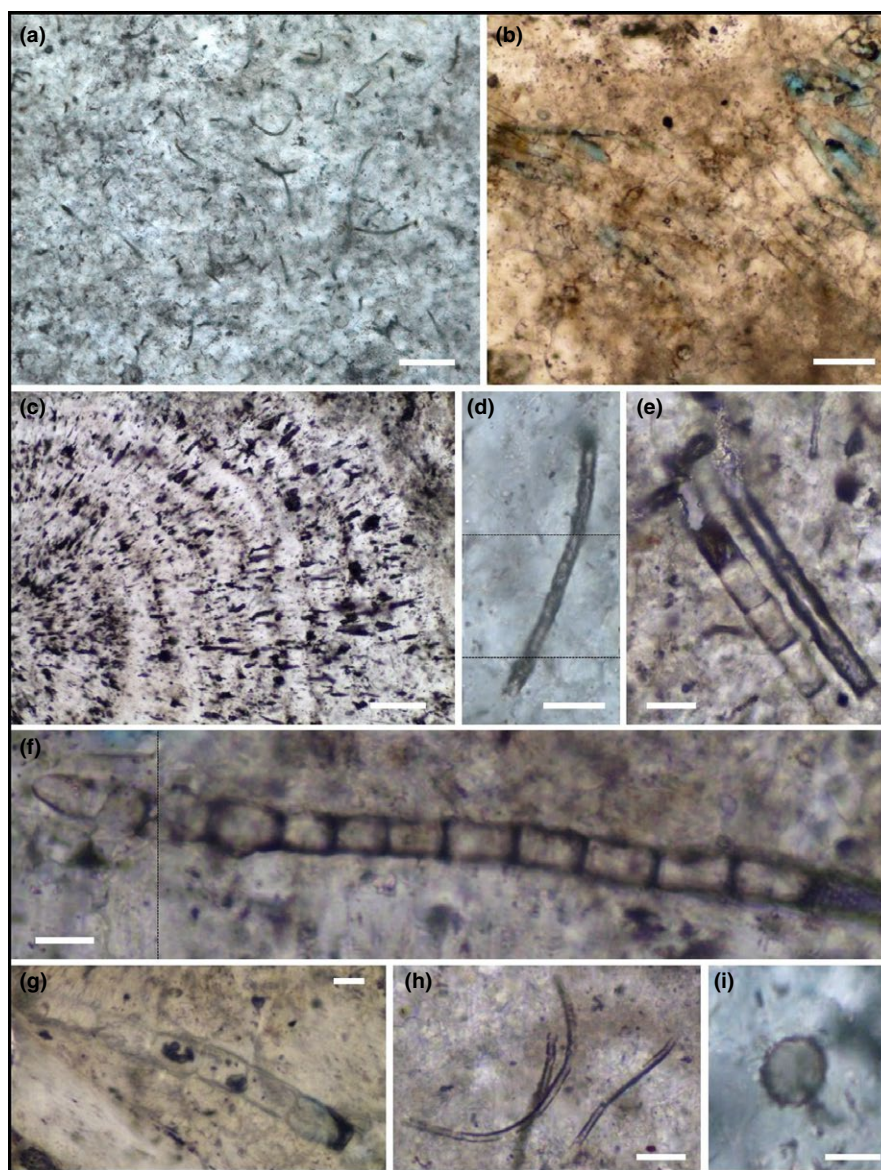


FIGURE 4 Fossilised bacteria within Mono Lake tufa chimneys. (a) Multiple type 1 filaments. (b) Cluster of approximately aligned segmented type 2 filaments. (c) Type 1 filaments aligned perpendicular to outward-radiating subcrystal boundaries. (d) Single Type 1 filament showing putative segmentation. (e) A Type 1 and Type 2 filament side by side. (f) Type 2 filament showing clear segmentation and potentially partially surrounded by a mineralised sheath. (g) Type 2 filament showing segmentation and potential remnants of cell contents. (h) Typical Type 1 empty sheaths. (i) Typical coccoid bacterium. Scale bars are 50 μm for (a–c) and 10 μm for (d–i). Dashed black lines indicate transition between images taken at different focal depths [Colour figure can be viewed at wileyonlinelibrary.com]

3 cm across (Figure 2c). Subhorizontal 15 cm-thick laminated calcitic sheets were observed between the pipes, binding them together (Figure 2b). Each chimney was found rooted in calcite-cemented lake sediment ("sand tufa"). Externally, the chimneys were encrusted in 20- to 50-cm-thick blankets of centimetre scale mesh-like networks of euhedral pseudomorphs after the low temperature hydrated CaCO_3 mineral ikaite, locally known as "thinolite tufa" (Russell, 1889; Shearman, McGugan, Stein, & Smith, 1989) (Figure 2a, d). Some of these pseudomorphs after ikaite are found on individual pipes that make up the chimneys, but only on outer pipe surfaces, which would have been exposed to lake water after the chimney had formed. Individual pseudomorphs of ikaite crystals in these "thinolite" blankets mostly measured around 5 cm in length, and crystals clustered together to form rosettes (Figure 2d).

3.1 | Petrography of chimney pipes

The walls of the c. 3 cm wide chimney pipes are mostly 0.5 to 1 cm thick, constructed of columns of calcite that grew radially around the c. 1 cm wide central conduit (Figure 3a–c). In places the calcite crystal columns that make up the pipe walls were cemented together, particularly towards the outside of the pipes. In zones closer to pipe conduits, however, the microsparry calcite columns were separated from each other by elongated voids running parallel to the column long axis (Figure 3a and b). Calcite crystal microspar columns may also branch and fan outwards resulting in millimetre to centimetre scale shrub-like morphologies (Figure 3d). When cut perpendicular to the crystal growth axes these radiating calcite fans appeared sub-circular. Between some of the pipes, fissure fills of clastic sediment were present.

3.2 | Microfossils within chimney pipes

Clusters of filaments, observed in thin sections under the optical microscope, are a major component of the chimneys: They are ubiquitous within the columnar to shrub-like calcite growths that make up the pipe walls (Figure 4a–c), with many thousands of specimens in a single thin section. Many of these filamentous structures were found rather randomly oriented, though others were oriented approximately perpendicular to outward-radiating subcrystal boundaries (Figure 4c).

Filaments may be divided into two main types, found together in the same thin sections, occupying the same niche. The most common (Type 1) have diameters in the range of c. 0.8 to 8 μm with modal peaks at c. 1 μm and c. 2.5 μm ($n > 500$) (Figure 4d, e, h). Type 1 filaments tend to be dark in colour, suggesting high organic content and poorly mineralised interiors. The Type 1 assemblage is dominated by empty sheaths (Figure 4a, h), although occasionally trichomes, some with putative segmentation, can be recognised (Figure 4d). Type 2 filaments have diameters in the range of c. 10 to 14.5 μm ($n > 100$), and comprise well-preserved trichomes with clear interior mineralisation. Trichome segmentation is present in almost all cases (Figure 4b, e–g) and potential remains of cell contents are sometimes observed (Figure 4g). Type 2 filament sheaths are either completely mineralised or were absent. Coccoids were also identified, ranging from 6.8 to 15 μm diameter ($n = 25$), but these were much rarer than filaments in the thin sections examined (Figure 4i). The morphologies of the filaments, including their size, segmentation and cases of trichomes inside sheaths, are consistent with their being fossils of cyanobacteria, as are found within modern Mono Lake spring systems (Kulp et al., 2008). Biomarker data reinforces this interpretation (see below

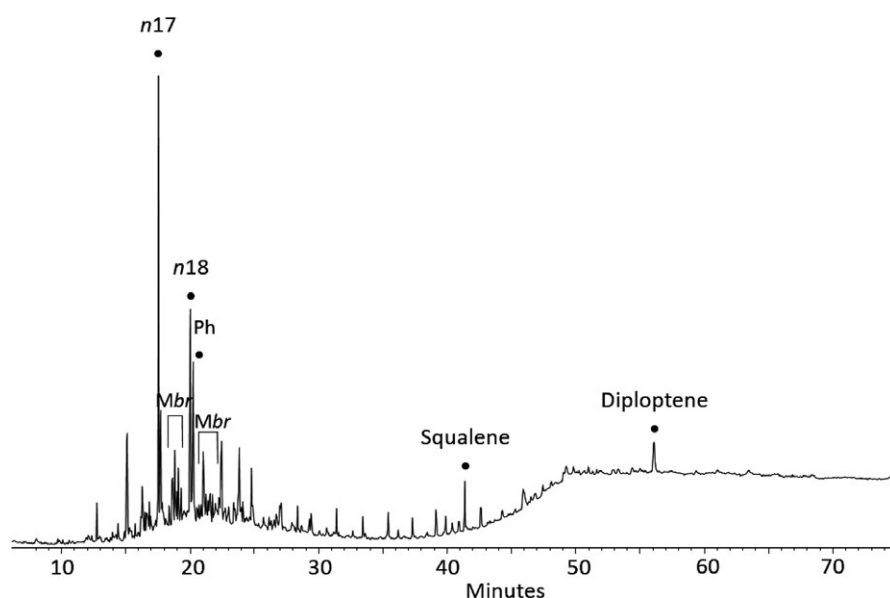
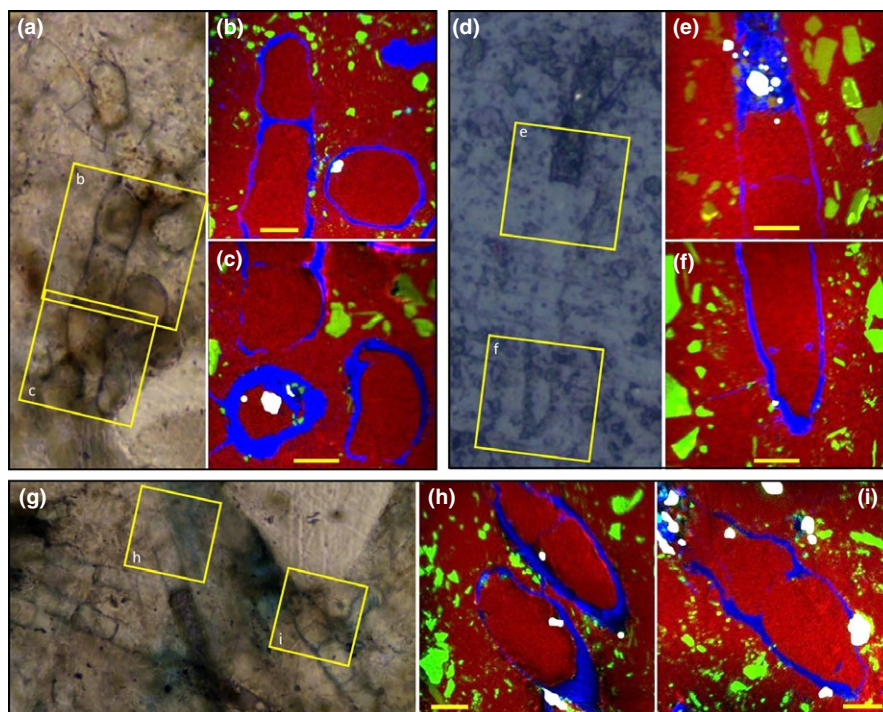


FIGURE 5 An 85 + 189 m/z ion chromatogram for a Mono City chimney pipe specimen. n17 = C_{17} n -alkane, Ph = phytane, Mbr = methylbranched alkane. This is consistent with the presence of cyanobacteria entombed within the Mono City chimney pipes

FIGURE 6 NanoSIMS analysis of Mono Lake tufa cyanobacteria and associated minerals. Transmitted (a,g) and reflected light (d) images of several segmented filamentous cyanobacteria from a Mono Lake tufa chimney pipe. In each case, the areas analysed by NanoSIMS are highlighted by the yellow boxes. (b-c; e-f; h-i) Four colour overlays of NanoSIMS ion images where blue represents organic material, green represents silicate grains, red represents calcite, and white represents contaminant SiC grains from polishing. Silicate grains are found surrounding, but very rarely within, the cyanobacteria. Scale bars are 5 μm for all NanoSIMS images [Colour figure can be viewed at wileyonlinelibrary.com]



and Figure 5). The microfossils are almost all in the inclusion-rich calcite of the chimney pipe walls, being rare to absent in the optically transparent calcitic pseudomorph after ikaite overgrowths of the thynolite blanket (Figure 3e).

3.3 | Tufa and microfossil chemistry

Bulk rock mineralogy was determined by XRD, with GC-MS for biomarkers of organic carbon entombed within the rock. The chemistry and ultrastructure of the filamentous microfossils and surrounding minerals were further investigated using a combination of nanoscale secondary ion mass spectrometry (NanoSIMS), scanning electron microscopy (SEM) and transmission electron microscopy (TEM).

The XRD data showed ~99% of chimney pipe rock to be calcite with an average magnesium content of 8.1(1)%. The remaining ~1% constituent of the rock was quartz (Supporting information Figure S1A-C). The Pleistocene Mono City chimneys are therefore significantly different in mineralogy from the younger, aragonitic, Holocene tufa mounds (Supporting information Figure S1D).

The hydrocarbon lipids obtained from a solvent extract of the Mono City chimney specimen (Figure 5) are similar to those of Arp et al. (1999) reported for Pyramid Lake and also to those found in endolithic and mat-forming cyanobacteria reported by Parnell et al. (2007). Typical features found in these stressed environments include a predominance of $n\text{-C}_{15}$ to C_{18} n -alkanes with a maximum at C_{17} , plus abundant monomethylalkanes and hydrocarbon hopenes such as diploptene (Figure 5). More generally it has been known for some time (Han, McCarthy, Calvin, & Benn, 1968; Thiel, Merz-Preiß, Reitner, & Michaelis, 1997) that abundant $n\text{-C}_{17}$ and monomethylalkanes (Shiea, Brassell, & Ward, 1990), can be found in photosynthetic

cyanobacteria. This is entirely consistent with the specimen petrography.

Filaments identified in the chimney pipe wall thin sections are highlighted particularly well in carbon and nitrogen NanoSIMS ion maps, with trichome segmentation in Type 2 filaments notable in several cases (Figure 6). Carbon and nitrogen are also frequently found with a very patchy distribution in places outside the trichomes (Figures 6-9) and are here interpreted as degraded extracellular organic material (EOM) from cyanobacterial sheaths and biofilms. This preserved "EOM" can be distinguished in the NanoSIMS data from potential epoxy resin contamination as the latter lacks nitrogen, so its $^{12}\text{C}^{14}\text{N}^-/^{24}\text{C}_2^-$ ratio is significantly less than the $^{12}\text{C}^{14}\text{N}^-/^{24}\text{C}_2^-$ ratios for cell walls or potential EOM (Supporting information Figure S2). Alternatively, this organic carbon could be interpreted as escaped cell contents or degrading cell walls, but an EOM interpretation is the most parsimonious explanation. NanoSIMS, SEM-EDS and TEM-EDS maps of Si show abundant silicate nanograins surrounding many of the Type 1 and Type 2 filaments, spatially associated with the C and N (detected by NanoSIMS and/or TEM) that can be interpreted as fossilised EOM (Figure 6b-c, e-f, h-i; Figure 7c, i-l; Figure 8b; Figure 9). These silicates have rather variable compositions and include (in order of abundance) quartz, K-Na-rich aluminosilicate (cf. alkali feldspar), plus Fe- and Mg-rich aluminosilicates (cf. chlorite group) (Figures 8 and 9). Silicates were only exceptionally rarely found in the interior of the filaments, and in these few cases, they were very close to the cell wall. In most observed cases filament interiors were filled solely with calcite. In one examined Type 2 filament, a Mn-Fe-rich carbonate mineral was observed within and just exterior to a cell wall (Figure 7a, e-f), while in one examined Type 1 filament

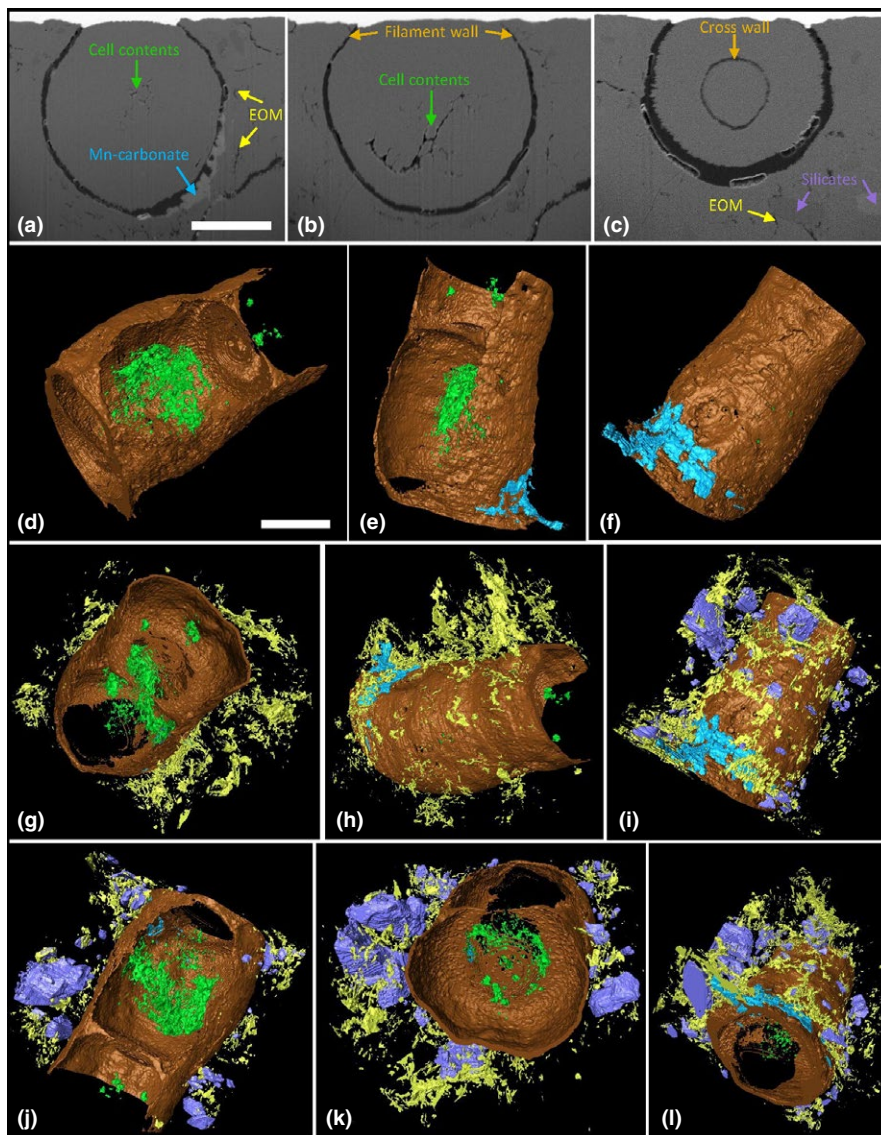


FIGURE 7 Three-dimensional analysis of fossilised cyanobacteria from Mono Lake tufa chimney pipes. (a-c) SEM-BSE images of a series of cross sections through a fossilised cyanobacterium. The different components of the cyanobacterium and associated minerals are labelled (based on correlative evidence from EDS and NanoSIMS maps), and the uniform mid-grey material making up most of the field of view is calcite. (d-l) 3D reconstructions of the cyanobacterium and associated minerals. Filament walls and cross walls are shown in brown, organic cell contents in green, inferred extracellular polymeric substances (EOM) in yellow, silicate minerals in purple and Mn-carbonate in blue. The remainder of each field of view (here made transparent black) is calcite. In reconstructions (d-f), only cell walls, organic cell contents and the Mn-carbonate mineral are shown for clarity; in (g-h), the EOM has been added to the reconstruction; while in (i-l), all components are shown, demonstrating the close spatial association of silicate minerals and EOM. Scale bar in (a) is 5 μm and applies to (a-c), and scale bar in (d) is also 5 μm and applies to (d-l) [Colour figure can be viewed at wileyonlinelibrary.com]

a Mn-Ti-Fe-rich carbonate was observed partially replacing the filament wall (Figure 9).

A rare subpopulation of Si-rich grains were found in close association with organic cell wall material; these comprise SiC and are laboratory contamination, having been introduced during polishing of the thin sections. These can easily be discriminated from true silicate minerals by their characteristic Si and C chemistry and lack of other elements (e.g., O) found in silicate minerals (Figure 6, white grains) and have been eliminated from further discussions.

3.4 | 3D microfossil morphology and mineral distribution

A three-dimensional reconstruction of a Type 2 fossil filament was produced from stacked SEM-BSE images captured during sequential focussed ion beam milling (see materials and methods). The reconstruction, correlated with SEM-EDS and NanoSIMS ion maps, reveals carbonaceous cell walls and cell dividing cross walls of a

filamentous cyanobacterium (Figure 7a-c, black; Figure 7d-l, brown). Some internal cell contents are remarkably fossilised, preserved as organic carbon structures encased in calcite (Figure 7d-l, green). The reconstruction emphasises that the interior of the cells are preserved entirely in calcite and lack inclusions of other grains. In one region an external cell wall is directly associated with an Mn-Fe-rich carbonate mineral (Figure 7e-f, h-l, blue). Silicate minerals are again shown to be spatially associated with partially degraded EOM surrounding the cells (Figure 7c, i-l, silicates in purple, EOM in yellow).

4 | DISCUSSION

4.1 | Temporal environmental changes

Some aspects of the chimneys appear to be entirely abiotic in origin: For example, the thinolite around the outside of the chimney and in places on the outsides of the central pipes very likely formed via recrystallisation of ikaite to calcite. This process is

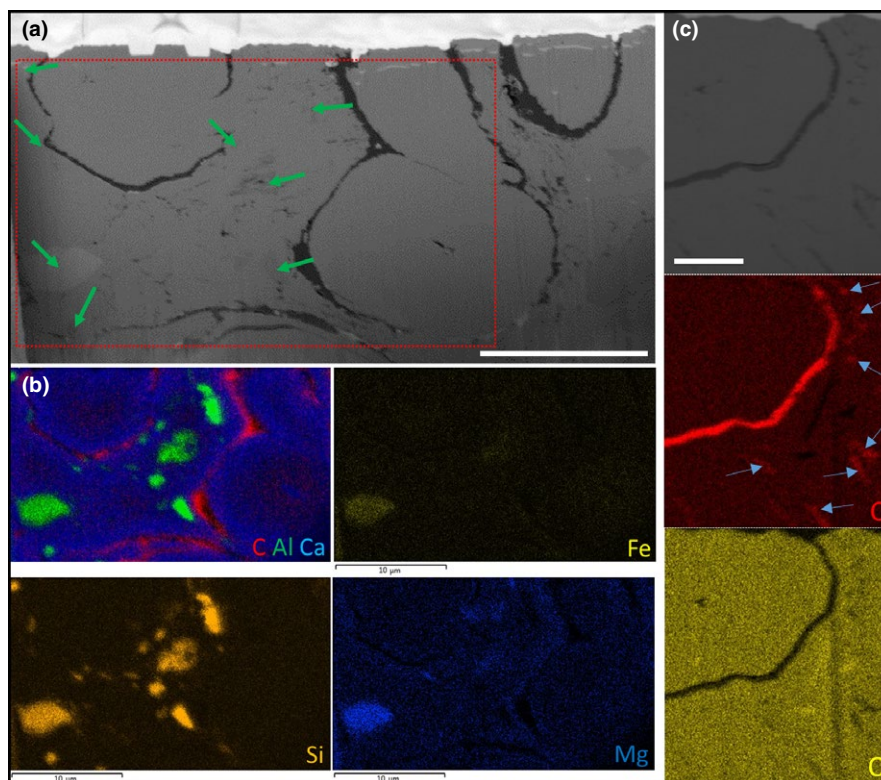


FIGURE 8 SEM-EDS analysis of the distribution of silicates and organic carbon around Mono Lake tufa cyanobacteria. (a) SEM-BSE image of a cross section through at least three Type 2 cyanobacteria. Note organic cell walls (black) and wispy extracellular organic material (EOM; also black). Red box shows area analysed in (b) and green arrows point to examples of silicates. (b) SEM-EDS elemental maps of carbon, aluminium and calcium (shown as RGB 3 colour overlay), plus iron, silicon and magnesium showing the close association of organic material and various silicate grains. Scale bars are 10 μm . (c) SEM-BSE image of a further Type 2 cyanobacterium with SEM-EDS elemental maps of carbon (red) and oxygen (yellow); both the cell wall and the wispy black material seen in the BSE image have elevated carbon contents (arrows) compared with the background carbonate mineral. Scale bar is 2 μm [Colour figure can be viewed at wileyonlinelibrary.com]

accompanied by a significant volume decrease, explaining the extreme porosity of the mesh-like thinolite networks (Shearman et al., 1989). That the ikaite formed a blanket covering of the chimneys suggests a change in environmental conditions, probably including a drop in lake water temperature, at some time following chimney development (Shearman et al., 1989). Suggestions of temporal environmental changes affecting carbonate mineral fabric are entirely consistent with the early observations of Russell (1889) who first noted that thinolite was only found at higher elevations around the lake.

A further environmental change is apparent in our new data: The dominance of high-Mg calcite within the Pleistocene deposits of the Mono City chimneys contrasts with aragonite (Supporting information Figure S1) and Mg-silicate (Souza-Egipsy et al., 2005) mineralogy of the younger Holocene mounds. Unfortunately, it is not possible for us to conclusively demonstrate co-occurrence of Mg-Si phases and aragonite because the samples we analysed were free of this material, and Souza-Egipsy et al. (2005) did not present crystallographic data. Rather, they assumed that Ca, O, C phases identified by EDS were low-Mg calcite: It seems likely that this was in fact aragonite. Calcite solubility is known to increase as fluid Mg/

Ca ratios are raised (Davis, Dove, & De Yoreo, 2000), such that rising Mg/Ca in the lake water sometime after the Mono City chimneys had formed could itself cause a change in the precipitating carbonate mineral from Pleistocene calcite to Holocene aragonite. Mg/Ca in spring and runoff waters within the Mono region range from 0.04 to 1, whereas lake waters are always >1 (Table 1) indicating that Ca is consumed selectively over Mg. This scavenging of Ca will be inversely proportional to the alkalinity (due to combined influence on the saturation product) and therefore likely inversely proportional to the lake level via dilution. Enhanced scavenging of Ca relative to Mg during lake lowstands will raise Mg/Ca during these time intervals, favouring aragonite precipitation. Reduced incorporation of Mg into aragonite due to very low $D_{\text{Mg-aragonite}}$ (Wassenburg et al., 2016) will cause a further rise in the lake water Mg concentration, ultimately triggering precipitation of non-carbonate Mg phases alongside aragonite. Hence, highstand high-Mg calcite deposition and lowstand aragonite + Mg-silicate precipitation can be seen as an inherent, thermodynamically controlled behaviour of Mono Lake, and similar hyperalkaline systems.

In contrast to the outer thinolite blanket, there is no petrographic evidence of any recrystallisation of the Pleistocene calcitic

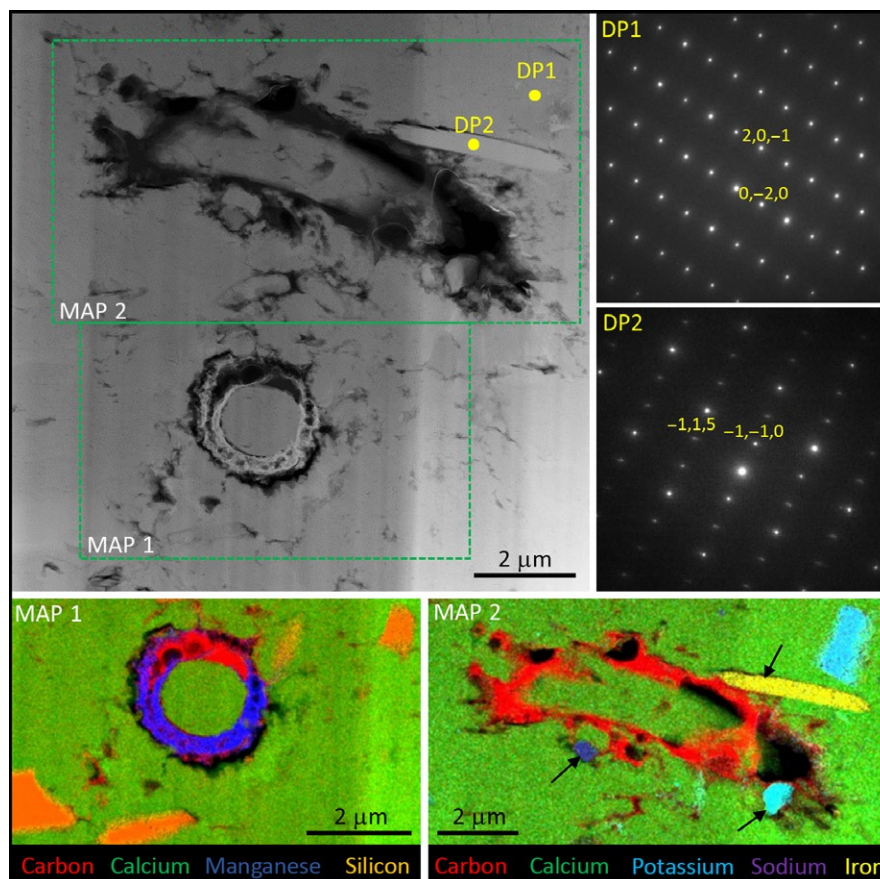


FIGURE 9 Chemistry of Type 1 filaments and surrounding minerals. High angle annular dark field scanning TEM image showing longitudinal and transverse sections, respectively, through two Type 1 filaments. The TEM-EDS elemental maps (bottom row) show that the filament walls and some extracellular material retain a carbonaceous composition (red). Some void space is present (black in these elemental maps), and this is not filled with epoxy resin. The lower filament is partly mineralised by an amorphous Mn-rich carbonate (dark blue; also containing minor Ti and Fe). Angular detrital aluminosilicate grains are closely associated with the filaments, and some are attached to the outer walls or extracellular organics of the upper filament (black arrows). Aluminosilicate grains are of variable composition with Na–K-rich varieties plus Fe–Mg-rich varieties. Selected area electron diffraction patterns show that the Na–K-rich grains are alkali feldspar (DP1 is consistent with anorthoclase viewed down the $[1,0,2]$ axis), while the Fe–Mg-rich grains are chlorite (DP2 is consistent with clinocllore viewed down the $[-5,5,-2]$ axis) [Colour figure can be viewed at wileyonlinelibrary.com]

chimney pipe walls (Figure 3). It is in these un-recrystallised and earlier formed calcite pipe walls that filamentous inclusions are found.

4.2 | Inclusions in the calcite

Biomarkers, NanoSIMS, SEM- and TEM-EDS elemental maps show the filamentous structures examined in pipe walls are clearly carbonaceous microfossils, while these techniques combined with light microscopy observations, together show the detailed spatial relationships between these fossil cyanobacterial filaments and calcite and silicate minerals.

Several mechanisms are plausible to explain the observed arrangement of silicates around filaments. First is an abiotic hypothesis, in which the microbes had no effect on silicate mineral distribution. However, here we might expect that any partially decayed cells would contain silicate grains that had been washed inside, and this was not observed. Rather, it seems that the organic

matter that we interpret as cell walls and EOM was spatially linked to the locations of the silicate grains (e.g., Figure 7). This leaves us with two hypotheses to assess: (i) that silicates could have been precipitated *in situ* via the metabolic activity of microbes (cf. Burne et al., 2014); or (ii) they could be fine detrital grains that have been trapped and bound by microbial EOM (cf. Reid et al., 2000).

4.3 | Microbial precipitation of silicate precursors versus detrital silicate grains

Authigenic microbial precipitation of silicates has recently been reported in a number of alkaline lakes (e.g., Lake Satonda (Arp, Reimer, & Reitner, 2003); Lake Clifton (Burne et al., 2014; Caselmann, 2005); Mexican Crater Lakes (Zeyen et al., 2015); Great Salt Lake (Pace et al., 2016); Lake Thetis (Caselmann, 2005; Wacey, Urosevic, Saunders, & George, 2017)), where it has been suggested that local increases of pH during oxygenic photosynthesis favour the precipitation of Mg–Si phases in and around cyanobacterial sheaths and

TABLE 1 Trace element concentrations of waters found in and around Mono Lake, California, in October 2014

Sample	Al	Ba	Ca	Cu	Fe	K	Li	Mg	Mn	Na	S	Si	Sr
Dechambeau hot spring	0.019	0.010	11.567	0.002	0.041	6.860	0.232	2.460	0.016	324.789	31.326	18.269	0.162
Lakeside spring	0.084	0.001	2.238	0.002	0.036	17.584	0.254	0.587	0.001	189.072	17.976	5.272	0.005
Lakewater at island	0.174	0.007	3.316	0.003	0.064	1434.739	11.855	12.861	0.012		1656.138	4.917	0.021
Lakewater at tower	0.046	0.007	3.025	0.004	0.065	1383.753	11.653	12.585	0.011		1704.602	5.092	0.017
Lakewater site 2	0.198	0.008	3.378	0.005	0.066	1461.272	12.069	12.946	0.012		1659.955	4.995	0.021
Lee Vining Creek	0.046	0.011	7.916	0.004	0.124	0.964	0.000	0.565	0.007	2.911	2.171	2.308	0.040
Mill Creek	0.116	0.021	8.526	0.011	0.226	3.466	0.000	0.857	0.011	9.287	3.843	3.093	0.038
Naval Beach spring	0.070	0.372	86.349	0.003	1.178	29.358	2.237	57.634	1.070	305.561	12.326	32.437	0.473
Rush creek	0.025	0.006	6.707	0.002	0.101	0.567	0.000	0.655	0.005	3.056	1.618	2.011	0.030
Simon spring 2	0.249	0.027	32.969	0.003	0.467	2.442	0.136	18.714	0.064	28.648	2.577	19.282	0.190
Simon spring 3	0.034	0.016	22.401	0.000	0.045	7.964	0.221	22.580	0.005	40.587	3.974	18.253	0.173
South Tufa lakeside spring	0.031	0.292	111.943	0.000	8.462	32.005	1.441	45.901	1.994	207.528	15.698	31.001	0.537
Warm spring near Dechambeau	0.075	0.022	17.041	0.003	0.187	2.017	0.000	0.680	0.022	4.892	4.265	1.397	0.052

in webs of EOM (e.g., Pace et al., 2016). In this scenario, carbonate minerals only precipitate (and often replace Mg-Si phases) at a later stage when the activities of CO_3 and Ca rise during heterotrophic degradation of cyanobacteria and their associated EOM. However, the chemistry and distribution of silicates in those aforementioned lake deposits are rather different to that observed in the calcitic Pleistocene Mono City chimneys. Electron diffraction patterns of individual silicates around the Mono City chimney filaments revealed compositions compatible with chlorite and feldspar (Figure 9), while bulk rock XRD also indicates minor quartz (Supporting information Figure S1). Few of the silicate grains examined contained abundant magnesium and none were pure Mg-Si phases such as the stevensite and kerolite phases previously reported from other alkaline lakes (Burne et al., 2014; Zeyen et al., 2015). Intriguingly, the lack of Mg-Si phases around the Pleistocene Mono chimney microbes is a notable difference from Mg-Si mineralised EOM reported from sand-cementing tufa of the modern Mono Lake shoreline (Souza-Egipsy et al., 2005).

It seems most likely that most if not all of the Pleistocene Mono City chimney silicates were detrital grains. In support of this interpretation, we note that many contained Al, which is often cited to indicate a detrital sediment component (e.g., Koning, Epping, & Van Rapphorst, 2002), and alkali feldspars cannot have formed *in situ* under lakewater pressures. Furthermore, the very patchy isolated pattern of grain distribution and their angular shapes (Figures 6, 8, 9) are in stark contrast to the generally massive nature of Mg-Si precipitates found replicating entire cyanobacterial sheaths or large volumes of thrombolites (Burne et al., 2014; Casemann, 2005; Wacey et al., 2017) in other alkaline lakes such as Lake Clifton and Lake Thetis in Western Australia.

While some authigenic chemical control of silicate precipitation by microbes, for example by attraction of cations including Al, K and Si to negatively charged compounds including uronic acids within the EOM (cf. Drews & Weckesser, 1982; Saunders, Rogerson, Wadhawan, Greenway, & Pedley, 2014), cannot be ruled out, the mechanism that best explains the morphologies, compositions and distribution of silicates in the Mono Lake chimneys is via trapping and binding by microbial EOM (cf. Reid et al., 2000).

In summary, there is no clear evidence that the individual and rather isolated silicate grains surrounding cyanobacterial filaments in the Mono Lake chimneys once formed a substantial and coherent template that could have acted as a precursor to the carbonate that is the dominant chimney constituent. That exceptionally preserved fossil microbial filaments are found in chimney calcite that is Mg-Si poor demonstrates that precursor silicate matrices are not prerequisites for cellular preservation of microbial life in alkaline lakes. Rather, formation of calcite in the Pleistocene Mono Lake (and elsewhere?) instead of coupled aragonite and amorphous Mg-Si phases seen in the Holocene Mono Lake mounds may dominantly reflect lower Mg/Ca ratios of the precipitating lake waters. Rising water levels in Mono Lake resulting in falling Mg/Ca ratios would likely cause the system to revert to precipitation of calcite, rather than aragonite and amorphous Mg-silicates.

4.4 | Intracellular carbonate minerals

Carbonate minerals dominate the pipes making up the Mono Lake chimneys and on the microscale are found both intracellularly and extracellularly in the examined groups of filamentous microfossils. Intracellular calcification of cyanobacteria was recently described from modern lacustrine microbialites of Lake Alchichica, Mexico (Couradeau et al., 2012). This took the form of spherical granules of benstonite ($\text{Sr}_{1.4}\text{Ba}_{2.7}\text{Mg}_{1.4}\text{C}_{10.9}\text{Ca}_6\text{Mg}(\text{CO}_3)_{13}$), averaging 270 nm in diameter that may have nucleated on carboxysomes. The authors of that study suggested that excess alkalinity produced during photosynthesis was trapped inside the cell by active precipitation of benstonite and not exported beyond the cell wall. However, the mineral fill of the fossil cyanobacteria of Mono Lake is calcite, which is neither rich in barium nor strontium, and no evidence for spherical granules was observed. There is some evidence of cell contents preserved within the cyanobacteria (Figure 7) but this takes the form of patchy degraded organic material and this likely represents the least labile intracellular material. The cause(s) and timing of carbonate mineral growth within such cells remain to be elucidated, though here could simply have been postmortem infiltration of the cell by a calcite-supersaturated fluid.

Manganese ($\pm\text{Fe}$ and Ti) carbonate is rare but when present is an amorphous phase based on electron diffraction, and distinctly associated with the cell wall itself (Figures 7a, 9). This was true of both Type 1 and Type 2 filaments. Bacterial cell walls are known to selectively accumulate Mn from surface waters (Konhauser, Fyfe, Ferris, & Beveridge, 1993). Association of Mn with the cell wall and not just the EOM suggests the mineralisation process involved more than a simple attraction of Mn cations to a negatively charged surface. The difference in Eh-pH conditions between the inside of the cell and mixed vent and lake waters outside the cell wall could explain this, as Mn^{2+} would be soluble inside the relatively low pH cell, but Mn carbonates would precipitate out at the redox boundary with high pH lake conditions (cf. Davison, 1993). This suggests that the rather rare Mn carbonates could have formed early.

4.5 | Biological influences on chimney growth

The majority of the calcite that makes up the chimneys developed outside the microbial filaments. By binding calcium the EOM will initially have inhibited calcite crystal formation, but on degradation this calcium will have been released (cf. Arp et al., 1999, 2001), and critically, tubular sheets of EOM from microbes that inhabited the zones around the rising vent waters will have been preferential sites of calcite crystal nucleation. Once calcite crystals had formed in the EOM of these mucilaginous, cohesive and quickly mineralised tubular sheets, there would be a lower activation energy to deposit more mass on these developing crystals than to generate new nuclei in the mixing water masses. Consequently, even if further chimney wall crystal growth operated via a largely abiotic process, this latter deposition could still be considered bio-influenced due to the control on location from the presence of biofilm. It is tempting to speculate

that the chimney form owes its origins in part to the presence of a biofilm. The rising chimney would present a stable substrate for microbial colonisation around likely the nutrient-rich (Table 1) and relatively well-illuminated waters. The result could be that tubular biofilm growth around rising spring waters leads to the formation of carbonate chimney pipes, and in turn, chimney growth assists biofilm development around the rising spring waters. Hence, the Mono City calcitic lacustrine chimneys seem broadly similar to other lacustrine hot spring carbonates (Arp et al., 1999), volcanic crater lake carbonates (Arp et al., 2003, 2012; Kazmierczak et al., 2011), tufa barrages (Emeis et al., 1987), chimney-like giant (40 m high) aragonitic microbialites of Lake Van (Kempe et al., 1991), simpler structured carbonate mounds of other alkaline lakes like those of Inner Mongolia (Arp et al., 1998) and the Ries crater, Germany (Pache, Reitner, & Arp, 2001), as well as siliceous lacustrine hydrothermal chimneys like those of Lake Taupo, New Zealand (Jones, de Ronde, Renaut, & Owen, 2007) in that the *location* of the calcitic chimneys has a primary abiotic control (fault controlled rising spring waters), but chimney *morphology* may well be microbially mediated. Calcitic tufa chimney systems could therefore be added to the list of macro-scale products of local environmental chemistry, physics and microbiology, with the biota exerting a strong control on fabric.

Support for microbial mediation of tufa chimneys comes from simpler structured tufa mounds like those of nearby Pyramid Lake (Arp et al., 1999) and Searle's Lake, California (Guo & Chafetz, 2012), where the mounds contain a macroscopic columnar stromatolite component plus microscopic calcite-cemented spheres, chains of beads, rods and filaments that strongly resemble bacteria (Guo & Chafetz, 2012). These observations led Guo and Chafetz (2012) to conclude that microbially induced calcification was the predominant process creating these deposits but they were unable to demonstrate a role for EOM. Similar observations come from the alkaline Lake Alchichica in Mexico where tubular chimney-like carbonate deposits (with central conduits similar to the Mono Lake material described herein) occur side by side with nodular and domal structures, all of which were interpreted as microbialites, with some preserving remnants of filamentous and coccoid cyanobacteria (Kazmierczak et al., 2011). These authors inferred that primary carbonate mineralisation was nucleated within EOM secreted by cyanobacterial biofilms.

5 | CONCLUSIONS

5.1 | Summary model for chimney growth

Our results show that the Mono City chimney pipes are packed full of fossil microbial filaments, with rare coccoids. These might be interpreted as centimetre-thick tubular ("rolled up") and vertically stacked calcified microbial mats. Evidently there was strong growth of a cyanobacterial biofilm around rising spring waters in the Pleistocene Mono Lake, and these microbes influenced tufa chimney fabric development at least at the nano- and micro-scales. Just exterior to the preserved microbial cells, quartz and

aluminosilicate grains are best taken as evidence that “sticky” EOM produced by cyanobacteria (and potentially other microbes) trapped and bound some clastic lake sediment grains. We cannot rule out that some of the aluminosilicates surrounding these filaments could have formed authigenically within the EOM (cf. Pace et al., 2016), although the chemistry of these grains, together with their angular shapes and isolated context in which several grains “float” in a calcite matrix, indicates these silicate grains are mostly detrital. A key finding is that Mg–Si phases were absent here, so this phase cannot be seen as a prerequisite for exquisite fossilisation of microbes in alkaline water settings (cf. Burne et al., 2014; Souza-Egipsy et al., 2005). Instead it seems likely that the calcitic nature of these Pleistocene chimneys reflects a low lake water Mg/Ca ratio, arising from dilution during phases of high lake level. Holocene aragonitic mounds coupled to Mg–Si phases (Souza-Egipsy et al., 2005) can then be explained by a rise in the lake water Mg/Ca ratio through time and are a predictable feature of the thermodynamics of this lake and any similar system.

Fossilisation of the microbes was likely related to the microbial EOM (cf. Arp et al., 1999) in that acidic extracellular substances will have stripped calcium from the rising vent waters, favouring calcite nucleation and subsequent organised calcite crystal growth at the vent site. Calcite mineralisation of the EOM and intracellular calcification were likely *postmortem* processes (cf. Arp et al., 2001, 2012). Adsorption of Mn to the organic carbon of the cell wall could also have happened *postmortem*, but petrography suggests this was an early process.

Summation of the evidence shows Pleistocene fossil tufa chimneys of Mono Lake are not solely the result of abiotic mixing between calcium-rich spring waters and alkaline lake waters (cf. Council & Bennett, 1993), although they were arranged linearly along an apparent fault line, showing that water chemistry and tectonics controlled chimney locations if not their fabrics. Rather, chimney fabric development was influenced at least at the nano- to microscale by microbes that colonised the fertile and relatively nutrient-rich vent sites. These findings have direct applicability to the search for ancient and extraterrestrial microbial life.

ACKNOWLEDGMENTS

Fieldwork was undertaken and samples collected under permit from CA State Parks and with the kind support of Mono Lake Tufa State Natural Reserve and the Mono Lake Committee. We acknowledge the facilities, scientific and technical assistance of the Australian Microscopy & Microanalysis Research Facility at the Centre for Microscopy Characterisation and Analysis, The University of Western Australia, a facility funded by the University, State and Commonwealth Governments. DW acknowledges funding from the Australian Research Council via the Future Fellowship scheme (FT140100321). BP Exploration Co. (GPTLIBPXIMB/NB/89573) is thanked for funding provided to the Universities of Hull and VU Amsterdam. SK acknowledges funding from the DAAD RISE internship programme. Three anonymous reviewers provided very helpful

comments, which improved the final manuscript. The authors declare no conflict of interests.

ORCID

Alexander Brasier  <http://orcid.org/0000-0001-6103-2848>

David Wacey  <http://orcid.org/0000-0002-7124-0701>

Mike Rogerson  <http://orcid.org/0000-0001-6016-0549>

REFERENCES

- Arp, G., Helms, G., Karlinska, K., Schumann, G., Reimer, A., Reitner, J., & Trichet, J. (2012). Photosynthesis versus exopolymer degradation in the formation of microbialites on the atoll of Kiribati, Republic of Kiribati, Central Pacific. *Geomicrobiology Journal*, 29, 29–65. <https://doi.org/10.1080/01490451.2010.521436>
- Arp, G., Hofmann, J., & Reitner, J. (1998). Microbial Fabric Formation in Spring Mounds (“Microbialites”) of Alkaline Salt Lakes in the Badain Jaran Sand Sea, PR China. *Palaos*, 13, 581–592. <https://doi.org/10.2307/3515349>
- Arp, G., Reimer, A., & Reitner, J. (2001). Photosynthesis-induced biofilm calcification and calcium concentrations in Phanerozoic oceans. *Science*, 292, 1701–1704. <https://doi.org/10.1126/science.1057204>
- Arp, G., Reimer, A., & Reitner, J. (2003). Microbialite formation in sea-water of increased alkalinity, Satonda Crater Lake, Indonesia. *Journal of Sedimentary Research*, 73, 105–127. <https://doi.org/10.1306/071002730105>
- Arp, G., Thiel, V., Reimer, A., Michaelis, W., & Reitner, J. (1999). Biofilm exopolymers control microbialite formation at thermal springs discharging into the alkaline Pyramid Lake, Nevada, USA. *Sedimentary Geology*, 126, 159–176. [https://doi.org/10.1016/S0037-0738\(99\)00038-X](https://doi.org/10.1016/S0037-0738(99)00038-X)
- Bischoff, J. L., Stine, S., Rosenbauer, R. J., Fitzpatrick, J. A., & Stafford, T. W. Jr (1993). Ikaite precipitation by mixing of shoreline springs and lake water, Mono Lake, California, USA. *Geochimica et Cosmochimica Acta*, 57, 3855–3865. [https://doi.org/10.1016/0016-7037\(93\)90339-X](https://doi.org/10.1016/0016-7037(93)90339-X)
- Bosak, T., Liang, B., Wu, T. D., Templer, S. P., Evans, A., Vali, H., ... Mui, J. (2012). Cyanobacterial diversity and activity in modern conical microbialites. *Geobiology*, 10, 384–401. <https://doi.org/10.1111/j.1472-4669.2012.00334.x>
- Burne, R. V., Moore, L. S., Christy, A. G., Troitzsch, U., King, P. L., Carnerup, A. M., & Hamilton, P. J. (2014). Stevensite in the modern thrombolites of Lake Clifton, Western Australia: A missing link in microbialite mineralization? *Geology*, 42, 575–578. <https://doi.org/10.1130/G35484.1>
- Caselmann, M. (2005). Rezente und subfossile mikrobialithe westaustralischer salzseen. Doctoral Thesis, Georg-August-Universität zu Göttingen. <http://ediss.uni-goettingen.de/handle/11858/00-1735-0000-0006-B32C-0>
- Cloud, P., & Lajoie, K. R. (1980). Calcite-impregnated defluidization structures in littoral sands of Mono Lake, California. *Science*, 210, 1009–1012. <https://doi.org/10.1126/science.210.4473.1009>
- Council, T. D., & Bennett, P. C. (1993). Geochemistry of ikaite formation at Mono Lake, California: Implications for the origin of tufa mounds. *Geology*, 21, 971–974. [https://doi.org/10.1130/0091-7613\(1993\)021<0971:GOIFAM>2.3.CO;2](https://doi.org/10.1130/0091-7613(1993)021<0971:GOIFAM>2.3.CO;2)
- Couradeau, E., Benzerara, K., Gerard, E., Moreira, D., Bernard, S., Brown, G. E. Jr, & Lopez-Garcia, P. (2012). An early-branching microbialite cyanobacterium forms intracellular carbonates. *Science*, 336, 459–462. <https://doi.org/10.1126/science.1216171>
- Davis, K. J., Dove, P. M., & De Yoreo, J. J. (2000). The role of Mg²⁺ as an impurity in calcite growth. *Science*, 290(5495), 1134–1137. <https://doi.org/10.1126/science.290.5494.1134>

- Davison, W. (1993). Iron and manganese in lakes. *Earth-Science Reviews*, 34, 119–163. [https://doi.org/10.1016/0012-8252\(93\)90029-7](https://doi.org/10.1016/0012-8252(93)90029-7)
- Dekov, V. M., Egueh, N. M., Kamenov, G. D., Bayon, G., Lalonde, S. V., Schmidt, M., ... Le Gall, B. (2014). Hydrothermal carbonate chimneys from a continental rift (Afar Rift): Mineralogy, geochemistry, and mode of formation. *Chemical Geology*, 387, 87–100. <https://doi.org/10.1016/j.chemgeo.2014.08.019>
- Della Porta, G. (2015). Carbonate build-ups in lacustrine, hydrothermal and fluvial settings: Comparing depositional geometry, fabric types and geochemical signature. *Geological Society, London, Special Publications*, 418, 17–68. <https://doi.org/10.1144/SP418.4>
- Drews, G., & Weckesser, J. (1982). In N. G. Carr, & B. A. Whitton (Eds.), *The biology of cyanobacteria* (pp. 333–358). London, UK: Blackwell.
- Dunn, J. R. (1953). The origin of the deposits of tufa in Mono Lake. *Journal of Sedimentary Petrology*, 23, 18–23. <https://doi.org/10.1306/D4269530-2B26-11D7-8648000102C1865D>
- Dupraz, C., Fowler, A., Tobias, C., & Visscher, P. T. (2013). Stromatolitic knobs in Storr's Lake (San Salvador, Bahamas): A model system for formation and alteration of laminae. *Geobiology*, 11, 527–548. <https://doi.org/10.1111/gbi.12063>
- Dupraz, C., Visscher, P. T., Baumgartner, L. K., & Reid, R. P. (2004). Microbe–mineral interactions: Early carbonate precipitation in a hypersaline lake (Eleuthera Island, Bahamas). *Sedimentology*, 51, 745–765. <https://doi.org/10.1111/j.1365-3091.2004.00649.x>
- Emeis, K. C., Richnow, H. H., & Kempe, S. (1987). Travertine formation in Plitvice National Park, Yugoslavia: Chemical versus biological control. *Sedimentology*, 34, 595–609. <https://doi.org/10.1111/j.1365-3091.1987.tb00789.x>
- Guo, X., & Chafetz, H. S. (2012). Large tufa mounds, Searles Lake, California. *Sedimentology*, 59, 1509–1535. <https://doi.org/10.1111/j.1365-3091.2011.01315.x>
- Han, J., McCarthy, E. D., Calvin, M., & Benn, M. H. (1968). Hydrocarbon constituents of the blue-green algae *Nostoc Muscurum*, *Anacystis nidulans*, *Phormidium luridum* and *Chlorogloea fritschii*. *Journal of the Chemical Society*, 1968C, 2785–2791.
- Jennings, C.W., Strand, R.G., & Rogers, T.H. (1977). Geologic map of California: California Division of Mines and Geology, scale 1:750,000.
- Jones, B., de Ronde, C. E. J., Renaut, R. W., & Owen, R. B. (2007). Siliceous sublacustrine spring deposits around hydrothermal vents in Lake Taupo, New Zealand. *Journal of the Geological Society of London*, 164, 227–242. <https://doi.org/10.1144/0016-76492005-102>
- Kazmierczak, J., Kempe, S., Kremer, B., Lopez-Garcia, P., Moreira, D., & Tavera, R. (2011). Hydrochemistry and microbialites of the alkaline crater lake Alchichica, Mexico. *Facies*, 57, 543–570. <https://doi.org/10.1007/s10347-010-0255-8>
- Kempe, S., Kazmierczak, J., Landmann, G., Konuk, T., Reimer, A., & Lipp, A. (1991). Largest known microbialites discovered in Lake Van, Turkey. *Nature*, 349, 605–608. <https://doi.org/10.1038/349605a0>
- Konhauser, K. O., Fyfe, W. S., Ferris, F. G., & Beveridge, T. J. (1993). Metal sorption and mineral precipitation by bacteria in two Amazonian river systems: Rio Solimoes and Rio Negro, Brazil. *Geology*, 21, 1103–1106. [https://doi.org/10.1130/0091-7613\(1993\)021<1103:MSAMPB>2.3.CO;2](https://doi.org/10.1130/0091-7613(1993)021<1103:MSAMPB>2.3.CO;2)
- Koning, E., Epping, E., & Van Rapphorst, W. (2002). Determining biogenic silica in marine samples by tracking silicate and aluminium concentrations in alkaline leaching solutions. *Aquatic Geochemistry*, 8, 37–62. <https://doi.org/10.1023/A:1020318610178>
- Kulp, T. R., Hoeft, S. E., Asao, M., Madigan, M. T., Hollibaugh, J. T., Fisher, J. C., ... Oremland, R. S. (2008). Arsenic(III) fuels anoxygenic photosynthesis in hot spring biofilms from Mono Lake, California. *Science*, 321, 967–970. <https://doi.org/10.1126/science.1160799>
- Li, H. C., & Ku, T. L. (1997). $\delta^{13}\text{C}$ – $\delta^{18}\text{O}$ covariance as a paleohydrological indicator for closed-basin lakes. *Palaeogeography, Palaeoclimatology, Palaeoecology*, 133, 69–80. [https://doi.org/10.1016/S0031-0182\(96\)00153-8](https://doi.org/10.1016/S0031-0182(96)00153-8)
- Pace, A., Bourillot, R., Bouton, A., Vennin, E., Galaup, S., Bundeleva, I., ... Visscher, P. T. (2016). Microbial and diagenetic steps leading to the mineralisation of Great Salt Lake microbialites. *Scientific Reports*, 6, 31495. <https://doi.org/10.1038/srep31495>
- Pache, M., Reitner, J., & Arp, G. (2001). Geochemical evidence for the formation of a large miocene “Travertine” mound at a sublacustrine Spring in a Soda Lake (Wallerstein Castle Rock, Nördlinger Ries, Germany). *Facies*, 45, 211–230. <https://doi.org/10.1007/BF02668114>
- Parnell, J., Bowden, S. A., Osinski, G. R., Lee, P., Green, P., Taylor, C., & Baron, M. (2007). Organic geochemistry of impactites from the Houghton impact structure, Devon Island, Nunavut, Canada. *Geochimica et Cosmochimica Acta*, 71(7), 1800–1819. <https://doi.org/10.1016/j.gca.2007.01.006>
- Pedley, H. M., Rogerson, M., & Middleton, R. (2009). Freshwater calcite precipitates from in vitro mesocosm flume experiments: A case for biomediation of tufas. *Sedimentology*, 56, 511–527. <https://doi.org/10.1111/j.1365-3091.2008.00983.x>
- Petroff, A. P., Beukes, N. J., Rothman, D. H., & Bosak, T. (2013). Biofilm growth and fossil form. *Physical Review X*, 3, 041012. <https://doi.org/10.1103/PhysRevX.3.041012>
- Reid, R. P., Visscher, P. T., Decho, A. W., Stolz, J. F., Bebout, B. M., Dupraz, C., ... DesMarais, D. J. (2000). The role of microbes in accretion, lamination and early lithification of modern marine stromatolites. *Nature*, 406, 989–992. <https://doi.org/10.1038/35023158>
- Rieger, T. (1992). Calcareous tufa formations. Searles Lake and Mono Lake: California. *Geology*, 45, 99–109.
- Russell, I.C. (1889). Quaternary history of Mono Valley, California. USGS 8th Annual Report for 1886–1887, p 261–394.
- Saunders, P., Rogerson, M., Wadhawan, J., Greenway, G., & Pedley, H. (2014). Mg/Ca ratios in freshwater microbial carbonates: Thermodynamic, Kinetic and Vital Effects. *Geochimica et Cosmochimica Acta*, 147, 107–118. <https://doi.org/10.1016/j.gca.2014.10.014>
- Scholl, D. W., & Taft, W. H. (1964). Algae, contributors to the formation of calcareous tufa, Mono Lake, California. *Journal of Sedimentary Petrology*, 34, 309–319.
- Shearman, D. J., McGugan, A., Stein, C., & Smith, A. J. (1989). Ikaite, $\text{CaCO}_3 \cdot 6\text{H}_2\text{O}$, precursor of the thnolites in the Quaternary tufas and tufa mounds of the Labontan and Mono Lake basins, western United States. *Geological Society of America Bulletin*, 101, 913–917. [https://doi.org/10.1130/0016-7606\(1989\)101<913:ICOPOT>2.3.CO;2](https://doi.org/10.1130/0016-7606(1989)101<913:ICOPOT>2.3.CO;2)
- Shiea, J., Brassell, S. C., & Ward, D. M. (1990). Mid-chain branched mono- and dimethyl alkane in hot spring cyanobacterial mats: A direct biogenic source for branched alkanes in ancient sediments? *Organic Geochemistry*, 15, 223–231. [https://doi.org/10.1016/0146-6380\(90\)90001-G](https://doi.org/10.1016/0146-6380(90)90001-G)
- Souza-Egipsy, V., Wierzbos, J., Ascaso, C., & Nealson, K. H. (2005). Mg-silica precipitation in fossilization mechanisms of sand tufa endolithic microbial community, Mono Lake (California). *Chemical Geology*, 217, 77–87. <https://doi.org/10.1016/j.chemgeo.2004.12.004>
- Stine, S. (1987). Mono Lake: The past 4000 years. Unpublished PhD thesis, University of California, Berkley. 614 pp.
- Thiel, V., Merz-Preiß, M., Reitner, J., & Michaelis, W. (1997). Biomarker studies on microbial carbonates: Extractable lipids of a calcifying cyanobacterial mat (Everglades, USA). *Facies*, 36, 163–172. <https://doi.org/10.1007/BF02536882>
- Wacey, D., Gleeson, D., & Kilburn, M. R. (2010). Microbialite taphonomy and biogenicity: New insights from NanoSIMS. *Geobiology*, 8, 403–406. <https://doi.org/10.1111/j.1472-4669.2010.00251.x>
- Wacey, D., Kilburn, M. R., Saunders, M., Cliff, J., & Brasier, M. D. (2011). Microfossils of sulfur metabolizing cells in ~3.4 billion year old rocks of Western Australia. *Nature Geoscience*, 4, 698–702. <https://doi.org/10.1038/ngeo1238>

- Wacey, D., Urosevic, L., Saunders, M., & George, A. D. (2017). Mineralization of filamentous cyanobacteria in Lake Thetis stromatolites, Western Australia: *Geobiology*, 16, 203–215 (in press).
- Walter, M. R., & Des Marais, D. J. (1993). Preservation of biological information in thermal spring deposits: Developing a strategy for the search for fossil life on Mars. *Icarus*, 101, 129–143. <https://doi.org/10.1006/icar.1993.1011>
- Wang, X., Ali, G., Hemming, S.R., Zimmerman, S.R.H., Stine, S.W., & Hemming, G. (2014). Lake level changes in the Mono Basin during the last deglacial period *American Geophysical Union, Fall Meeting 2014, abstract PP51D-1157*.
- Wassenburg, J., Scholz, D., Jochum, K. P., Cheng, H., Oster, J., Immenhauser, A., ... Breitenbach, S. F. M. (2016). Determination of aragonite trace element distribution coefficients from speleothem calcite–aragonite transitions. *Geochimica et Cosmochimica Acta*, 190, 347–367. <https://doi.org/10.1016/j.gca.2016.06.036>
- Zeyen, N., Benzerara, K., Li, J., Groleau, A., Balan, E., Robert, J.-L., ... Lopez-Garcia, P. (2015). Formation of low-T hydrated silicates in modern microbialites from Mexico and implications for microbial fossilization. *Frontiers in Earth Science*, 3, 64.
- Zimmerman, S. R. H., Hemming, S. R., Hemming, N. G., Tomascak, P. B., & Pearl, C. (2011). High resolution chemostratigraphic record of late Pleistocene lake-level variability, Mono Lake, California. *Geological Society of America Bulletin*, 123, 2320–2334. <https://doi.org/10.1130/B30377.1>

SUPPORTING INFORMATION

Additional supporting information may be found online in the Supporting Information section at the end of the article.

How to cite this article: Brasier A, Wacey D, Rogerson M, et al.

A microbial role in the construction of Mono Lake carbonate chimneys? *Geobiology*. 2018;16:540–555. <https://doi.org/10.1111/gbi.12292>